Electronic Supplementary Information

2D hexagonal assembly of a dipolar rotor with a close interval of 0.8 nm using a triptycene-based supramolecular scaffold

Takejiro Ogawa,[a,b] Fumitaka Ishiwari,*[a] Fatin Hajjaj,[a] Yoshiaki Shoji,[a,b,c] Takashi Kajitani,[a,d,e] Koji Yazawa,[f] Takahiro Ohkubo[g] and Takanori Fukushima*[a,b,c]

[a] Laboratory for Chemistry and Life Science, Institute of Innovative Research, Tokyo Institute of Technology, 4259 Nagatsuta, Midori-ku, Yokohama 226-8501, Japan.
[b] Department of Chemical Science and Engineering, School of Materials and Chemical Technology, Tokyo Institute of Technology, 4259 Nagatsuta, Midori-ku, Yokohama 226-8501, Japan.
[c] Research Center for Autonomous Systems Materialogy (ASMat), Institute of Innovative Research, Tokyo Institute of Technology, 4259 Nagatsuta, Midori-ku, Yokohama, Kanagawa, 226-8501, Japan
[d] Open Facility Development Office, Open Facility Center, Tokyo Institute of Technology, 4259 Nagatsuta, Midori-ku, Yokohama 226-8501, Japan.
[e] RIKEN SPring-8 Center, 1-1-1 Kouto, Sayo, Hyogo 679-5148, Japan.
[f] JEOL Ltd., 3-1-2 Musashino, Akishima, Tokyo, 196-8558, Japan.
[g] Department of Applied Chemistry and Biotechnology, Graduate School of Engineering, Chiba University, 1–33 Yayoi-cho, Inage-ku, Chiba 263-8522, Japan.

*To whom correspondence should be addressed.
E-mail: ishiwari@chem.eng.osaka-u.ac.jp (F.I.), fukushima@res.titech.ac.jp (T.F.)

Table of contents

1. Materials and methods

Unless otherwise stated, all commercial reagents were used as received. 10-ethynyl-1,8,13-tridodecyloxy triptycene was synthesized according to the procedure reported previously.[S1]

NMR spectroscopy measurements in solution were carried out on a Bruker model AVANCE-500 spectrometer (500.0 MHz for ^{1}H, 125.7 MHz for ^{13}C, and 470.5 MHz for ^{19}F). Chemical shifts (δ) are expressed relative to the resonances of the residual non-deuterated solvents for ^{1}H [$CDCl_3$: $^{1}H(\delta)$ = 7.26 ppm] and ^{13}C [$CDCl_3$: $^{13}C(\delta)$ = 77.16 ppm], and the resonance of CF_3CO_2H as an external standard for ^{19}F (CF_3CO_2H: $^{19}F(\delta)$ = –76.55 ppm). Absolute values of the coupling constants are given in Hertz (Hz), regardless of their sign. Multiplicities are abbreviated as singlet (s), doublet (d), triplet (t) and multiplet (m). Infrared (IR) spectra were recorded at 25 °C on a JASCO model FT/IR-6600ST Fourier-transform infrared spectrometer. High-resolution atmospheric pressure chemical ionization time of flight (APCI-TOF) mass spectrometry measurements were performed on a Bruker model microTOF II mass spectrometer. Differential scanning calorimetry (DSC) measurements were carried out on a Mettler–Toledo model DSC 1 differential scanning calorimeter, where temperature and enthalpy were calibrated with In (430 K, 3.3 J/mol) and Zn (692.7 K, 12 J/mol) standard samples in sealed Al pans. Heating and cooling profiles were recorded and analyzed using the Mettler–Toledo STARe software system. Thermogravimetric analysis (TGA) was performed on a SHIMADZU model TGA-50 analyzer.

2. Synthesis of compound 1

Under a nitrogen atmosphere, dry and degassed DMF (5 mL) and triethylamine (1.6 mL) were added to a mixture of 10-ethynyl-1,8,13-tridodecyloxy triptycene[S1] (165.8 mg, 0.20 mmol), $Pd(PPh_3)_2Cl_2$ (4.6 mg, 6.55 μmol), $Pd(PPh_3)_4$ (4.9 mg, 4.24 μmol), CuI (1.3 mg, 6.83 μmol), and 2,3-difluoro-1,4-diiodobenzene (32.91 mg, 0.09 mmol), and the resulting mixture was stirred at 70 °C for 24 h. After being cooled to 25 °C, the reaction mixture was diluted with chloroform (150 mL) and passed through a plug of Celite®. The filtrate was washed successively with a saturated aqueous solution of NH_4Cl and brine, dried over anhydrous Na_2SO_4, and evaporated to dryness under reduced pressure. The residue was recrystallized from hot chloroform to give **1** (91.5 mg, 0.05 mmol) as a white microcrystalline powder in 57% yield: ^{1}H NMR (500.0 MHz, $CDCl_3$, 25 °C): δ (ppm) 7.61 (d, J = 2.5 Hz, 2H), 7.43 (d, J = 7.5 Hz, 6H), 6.99 (dd, J = 8.2, 7.8Hz, 6H), 6.98 (s, 2H), 6.64 (d, J = 8.2 Hz, 6H), 3.99 (t, J = 6.4 Hz, 12H), 1.90–1.85 (m, 12H), 1.63–1.57 (m, 12H), 1.41–1.28 (br, 96H), 0.89 (t, J = 6.6 Hz, 18H). ^{13}C{^{1}H} NMR (125.7 MHz, $CDCl_3$, 50 °C): δ (ppm) 154.2, 152.0 (dd, J = 255.7, 14.7 Hz), 147.4, 133.5, 128.2, 125.7, 115.5, 114.5 (dd, J = 9.6, 5.2 Hz), 111.3, 93.9, 84.0, 69.4, 54.6, 32.9, 32.1, 30.0–29.9 (five peaks), 29.6, 26.3, 22.9, 14.2. ^{19}F{^{1}H} NMR (470.5 MHz, $CDCl_3$, 25 °C): δ (ppm) –133.3. FT-IR (KBr): ν (cm^{-1}) 2924, 2852, 1604, 1499, 1486, 1469, 1392, 1325, 1274, 1195, 1152, 1055, 784, 745. APCI-TOF mass: calcd. For $C_{122}H_{172}F_2O_6$ $[M]^+$: m/z = 1772.3151; found: 1772.3151. Anal. Calcd for $C_{122}H_{172}F_2O_6$: C, 82.66; H, 9.78; F, 2.14. Found: C, 82.71; H, 10.02; F, 2.14. The ^{1}H, ^{13}C{^{1}H}, ^{19}F{^{1}H} NMR spectra, FT-IR, high-resolution APCI-TOF mass spectra, and TGA profile of **1** are shown in Figures S1, S2, S3, S4, S5, and S6, respectively.

3. Powder X-ray diffraction (PXRD) measurements

PXRD patterns were measured using a Rigaku model NANOPIX X-ray diffractometer (Cu $K\alpha$, wavelength of the X-ray beam λ = 1.54 Å) equipped with a HyPix-6000 detector. Variable-

temperature (VT) synchrotron PXRD patterns were measured using the BL45XU beamline (λ = 1.0 Å) at SPring-8 (Hyogo, Japan) equipped with a Pilatus3X 2M (Dectris) detector. The scattering vector ($q = 4\pi\sin\theta/\lambda$) and the position of the incident X-ray beam on the detectors were calibrated using several orders of layer reflections from silver behenate (d = 58.380 Å), where 2θ refers to the scattering angle. The sample-to-detector distances were *ca.* 90 mm (NANOPIX) and 0.40 m (BL45XU). The obtained diffraction patterns were integrated along the Debye-Scherrer ring to afford 1D intensity data using the Rigaku 2DP (NANOPIX) and FIT2D (BL45XU) software. The cell parameters were refined using the CellCalc ver. 2.10 software.[S2]

4. Solid-state ^{19}F-MAS NMR measurements

Solid-state ^{19}F-MAS NMR measurements of an as-recrystallized sample of **1** were carried out on a JEOL model JNM-ECA400 (^{19}F Larmor frequency: 376.17 MHz) spectrometer. VT solid-state ^{19}F-MAS NMR measurements of a thermally treated sample of **1** having the 2D+1D structure were carried out on a JEOL model JNM-ECZL500G (11.75 T) spectrometer (^{19}F Larmor frequency: 470.62 MHz). Powder samples of **1** were packed in a zirconia rotor and spun at 17.2 (JNM-ECA400) and 15.0 (JNM-ECZL500G) kHz for the as-recrystallized and thermally treated samples, respectively, using a 3.2-mm probe. For the thermally treated sample, ^{19}F single-pulse spectra were recorded with a $\pi/2$-pulse duration of 2.5 μs using the depth2 background suppression method. The values of spin-lattice relaxation time in the laboratory frame (T_1) and in the rotating frame ($T_{1\rho}$) were obtained by the saturation-recovery and spin-lock methods (the spin-lock frequency: 50 kHz), respectively. Representative fittings are shown in Figures S8, S10, and S11. The ^{19}F chemical shift was referenced to $CFCl_3$ (δ = 0 ppm) using a secondary reference of the CF_2 signal of PTFE (δ = –122 ppm).[S3] For the VT measurements, the sample temperature was calibrated using $Pb(NO_3)_2$ as an NMR thermometer.[S4,S5]

5. Computational methods

Energy calculations for the rotational motion of the rotor unit in the 2D hexagonal triptycene assembly were carried out using Density Functional Theory (DFT). To reduce the computational cost, we employed a simplified molecular model (**1'**), in which the dodecyloxy groups of **1** are replaced by hydrogen atoms (Fig. 8a). Geometrical optimization of **1'** in vacuum was performed at the ωB97XD/6-31+G(d,p) level of theory using the Gaussian16 program package.[S6] Optimized **1'** molecules were placed in a unit cell of a hexagonal lattice (a = 0.7961 nm, c = 3.5 nm) to form a 2D nested hexagonal packing (Fig. 8a). The value of a was taken from that observed for the 2D+1D assembly of **1** at 25 °C. The length of the c-axis (3.5 nm) results from a setup with a 1.5 nm thick slab layer between the 2D hexagonal triptycene sheets, so that interlayer interactions can be neglected. All atomic positions in the hexagonal cell were then optimized while the cell dimensions were fixed, using the Vienna Ab initio Simulation Package (VASP)[S7–S9] and plane-wave basis functions with three-dimensional periodic boundary conditions. The Perdew–Burke–Ernzerhof (PBE) exchange–correlation functional was used in the generalized gradient approximation.[S10] A commonly used correction for van der Waals interactions was applied to the system using the dispersion-corrected DFT (DFT-D3) of Grimme *et al.*[S11] The numbers of explicit valence electrons used in the pseudopotentials were 1, 4 and 7 for H, C and F ions, respectively. The energy cutoff in the expansion of the plane waves was set at 9224.4 kcal/mol (400 eV), which was requested from the pseudopotentials used. The convergence for the self-consistent field (SCF) loop were 23.061×10^{-5} kcal/mol

(10^{-5} eV). The system was treated as an insulator, and the *k*-point was set to 2×2×1 *k*-point mesh. The atomic positions were optimized until the total energy was less than 23.061×10^{-5} kcal/mol (10^{-5} eV) between two ionic steps. A 2×2×1 super-cell ($Z = 4$) was constructed, and the rotor unit of **1'** molecule, placed at the center of the 2D hexagonal lattice, was rotated manually in 5-degree increments (rotational angle θ = 0–360°, Fig. 8a) while the angle of the other rotor units remained fixed. The total energies of the 72 generated structures were obtained by single-point DFT calculations with 23.061×10^{-5} kcal/mol (10^{-5} eV) convergence of the SCF loop. Input structures and computational results were deposited in Zenodo: https://zenodo.org/records/11201814.

6. Supplementary references

S1. F. K. C. Leung, F. Ishiwari, T. Kajitani, Y. Shoji, T. Hikima, M. Takata, A. Saeki, S. Seki, Y. M. A. Yamada and T. Fukushima, *J. Am. Chem. Soc.,* 2016, **138**, 11727–11733.

S2 H. Miura, *J. Crystallogr. Soc. Jpn.* 2003, **45**, 145–147.

S3 T. R. Dargaville, G. A. George, D. J. T. Hill, U. Scheler and A. K. Whittaker, *Macromolecules*, 2002, **35**, 5544–5549.

S4. T. Takahashi, H. Kawashima, H. Sugisawa and T. Baba, *Solid State Nucl. Magn. Reson.*, 1999, *15*, 119–123.

S5. A. Bielecki and D. P. Burum, *J. Magn. Reson. Ser. A*, 1995, **116**, 215–220.

S6. Gaussian 16, Revision C.01, M. J. Frisch, G. W. Trucks, H. B. Schlegel, G. E. Scuseria, M. A. Robb, J. R. Cheeseman, G. Scalmani, V. Barone, G. A. Petersson, H. Nakatsuji, X. Li, M. Caricato, A. V. Marenich, J. Bloino, B. G. Janesko, R. Gomperts, B. Mennucci, H. P. Hratchian, J. V. Ortiz, A. F. Izmaylov, J. L. Sonnenberg, D. Williams-Young, F. Ding, F. Lipparini, F. Egidi, J. Goings, B. Peng, A. Petrone, T. Henderson, D. Ranasinghe, V. G. Zakrzewski, J. Gao, N. Rega, G. Zheng, W. Liang, M. Hada, M. Ehara, K. Toyota, R. Fukuda, J. Hasegawa, M. Ishida, T. Nakajima, Y. Honda, O. Kitao, H. Nakai, T. Vreven, K. Throssell, J. A. Montgomery, Jr., J. E. Peralta, F. Ogliaro, M. J. Bearpark, J. J. Heyd, E. N. Brothers, K. N. Kudin, V. N. Staroverov, T. A. Keith, R. Kobayashi, J. Normand, K. Raghavachari, A. P. Rendell, J. C. Burant, S. S. Iyengar, J. Tomasi, M. Cossi, J. M. Millam, M. Klene, C. Adamo, R. Cammi, J. W. Ochterski, R. L. Martin, K. Morokuma, O. Farkas, J. B. Foresman, and D. J. Fox, Gaussian, Inc., Wallingford CT, **2016**.

S7. J. Hafner, *J. Compt. Chem.*, 2008, **29**, 2044–2078.

S8. G. Kresse, J. Hafner, *Phys. Rev. B.*, 1993, **47**, 558–561.

S9. G. Kresse, J. Furthmüller, *Phys. Rev. B*, 1996, **54**, 11169–11186.

S10. J. P. Perdew, K. Burke, M. Ernzerhof, *Phys. Rev. Lett.*, 1996, **77**, 3865–3868.

S11. S. Grimme, S. Ehrlich, L. Goerigk, *J. Comput. Chem.*, 2011, **32**, 1456–1465.

S12. R. Kubo and K. Tomita, *Phys. Soc. Jpn.*, 1954, **9**, 888–919.

7. Supplementary figures

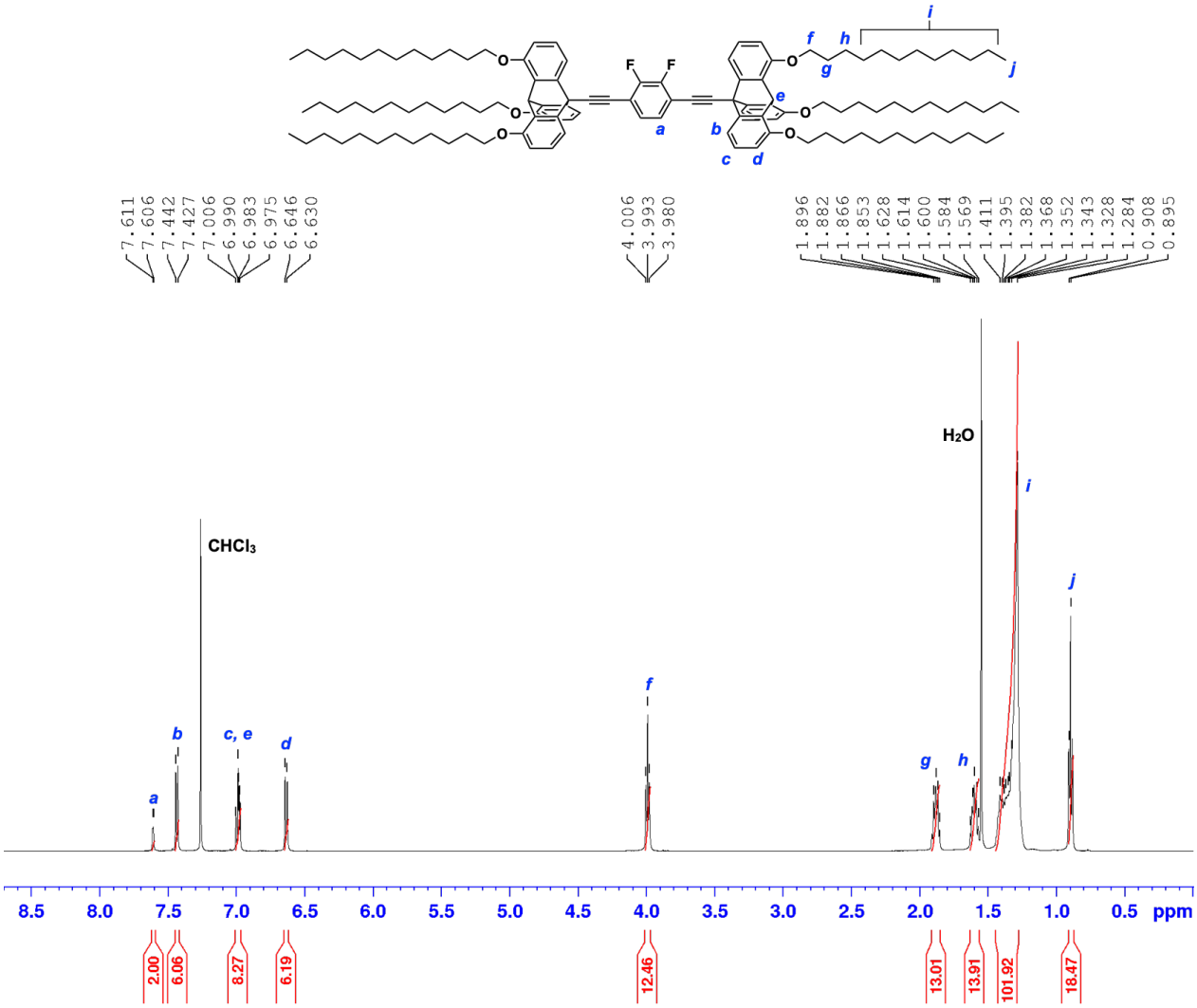

Fig. S1. ^{1}H NMR spectrum (500.0 MHz) of **1** in $CDCl_3$ at 25 °C.

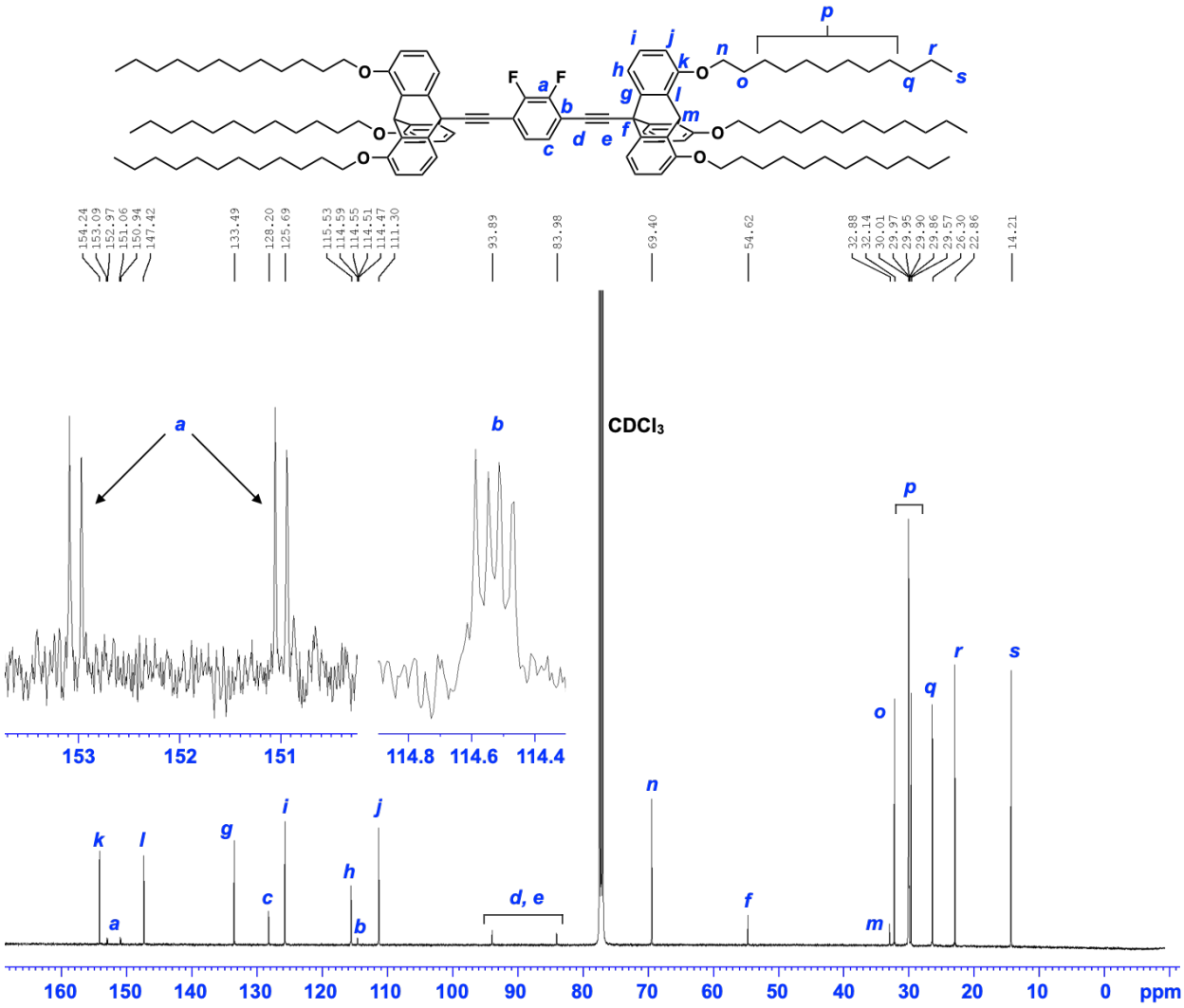

Fig. S2. $^{13}C\{^{1}H\}$ NMR spectrum (125.7 MHz) of **1** in $CDCl_3$ at 50 °C.

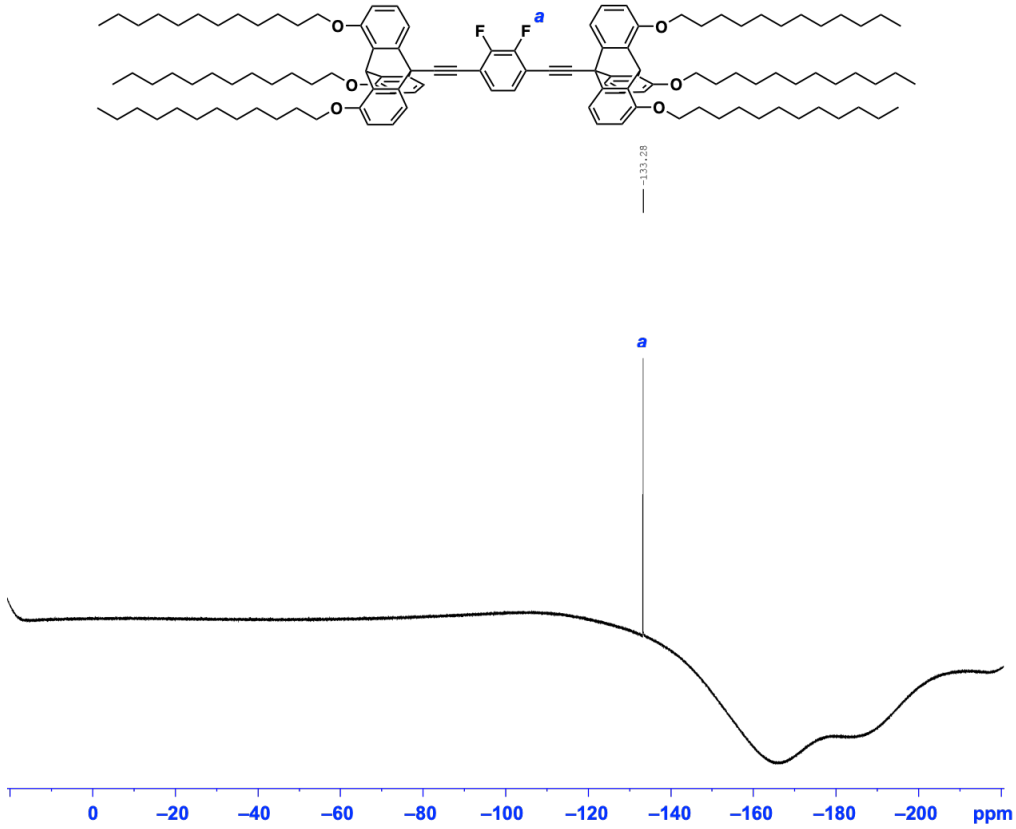

Fig. S3. $^{19}F\{^{1}H\}$ NMR spectrum (470.5 MHz) of **1** in $CDCl_3$ at 25 °C.

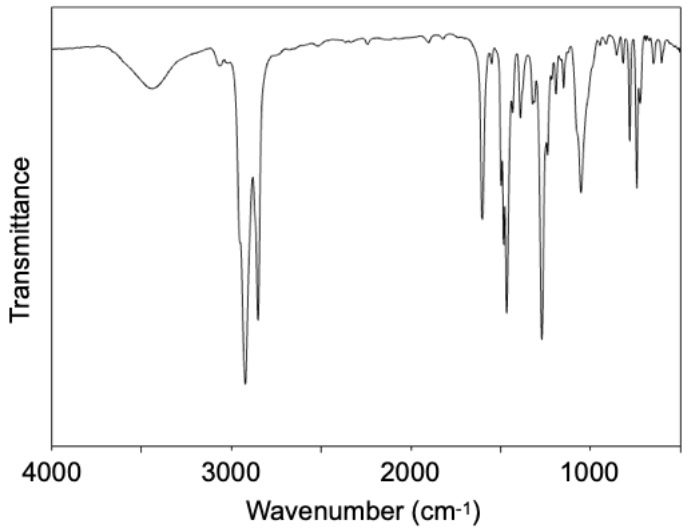

Fig. S4. FT-IR spectrum of **1** (KBr) at 25 °C.

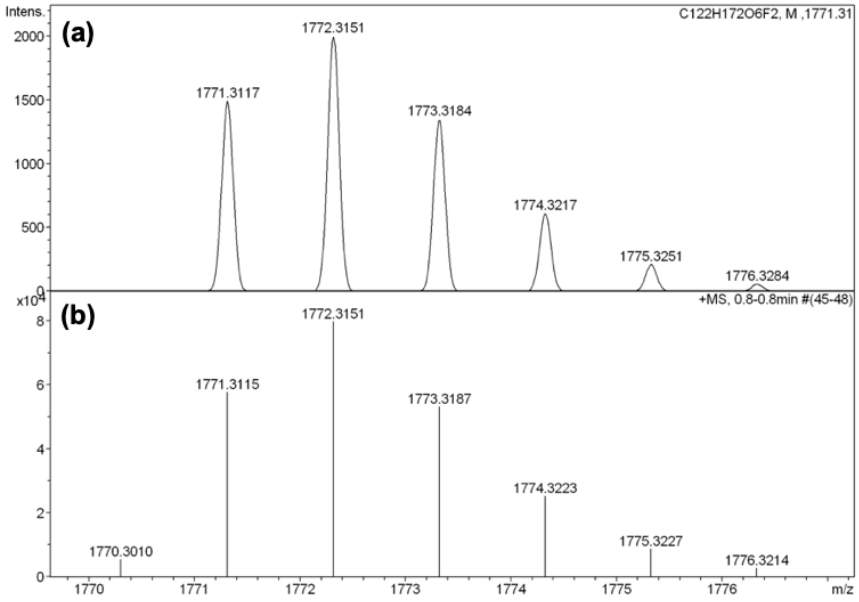

Fig. S5. (a) Simulated and (b) observed high-resolution APCI-TOF-mass spectrum of **1**.

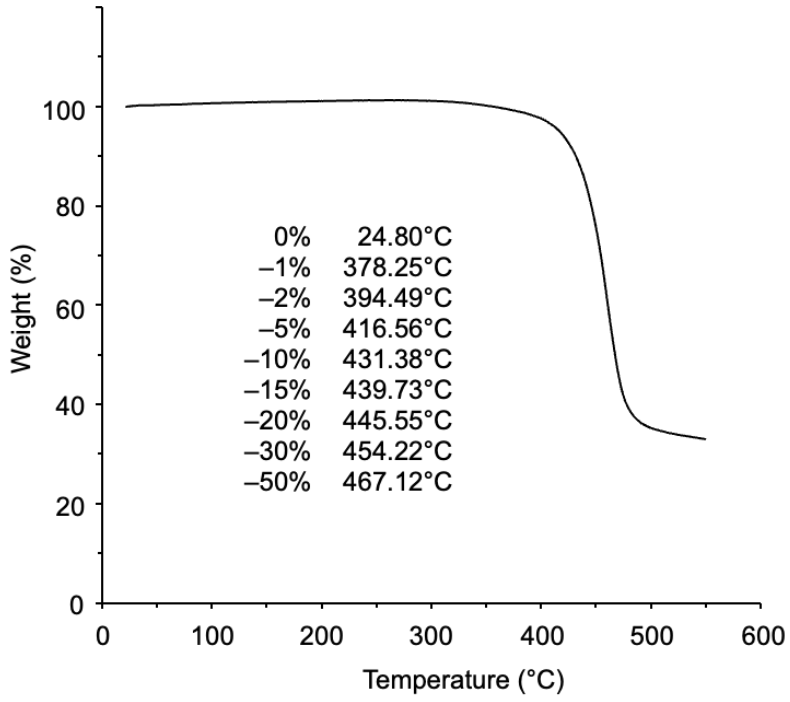

Fig. S6. TGA profile of **1** under N_2. Heating rate = 10 °C/min.

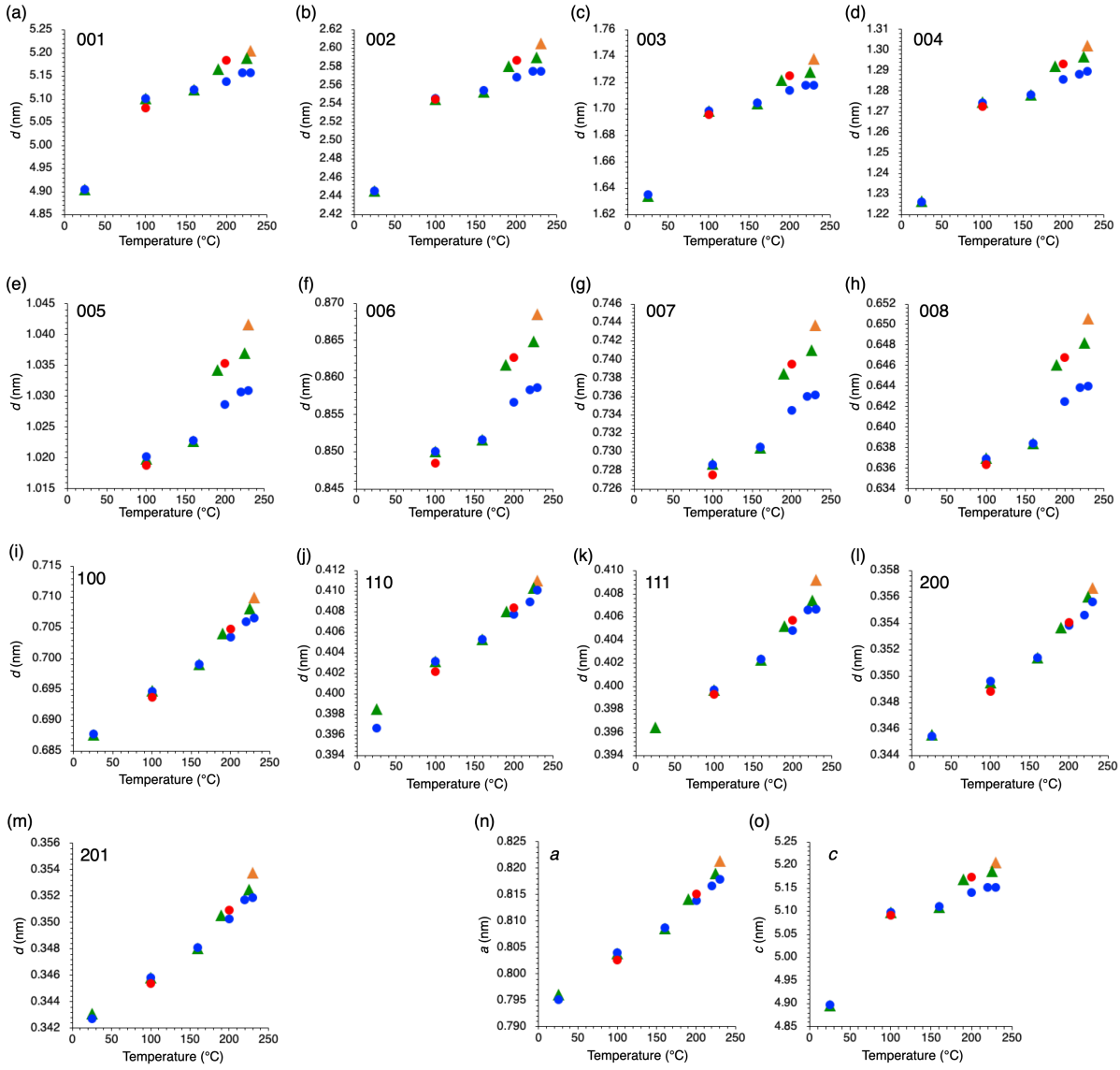

Fig. S7. Temperature-dependence of *d*-spacings for diffraction peaks indexed as (a) 001, (b) 002, (c) 003, (d) 004, (e) 005, (f) 006, (g) 007, (h) 008, (i) 100, (j) 110, (k) 111, (l) 200, and (m) 201, as well as cell parameters (n) *a* and (o) *c*, for the PXRD data presented in Fig. 4, observed during the first heating (orange triangles)/cooling (green triangles) and the second heating (red circles)/cooling (bule circles) cycles. See also Table S1 for the peak assignments.

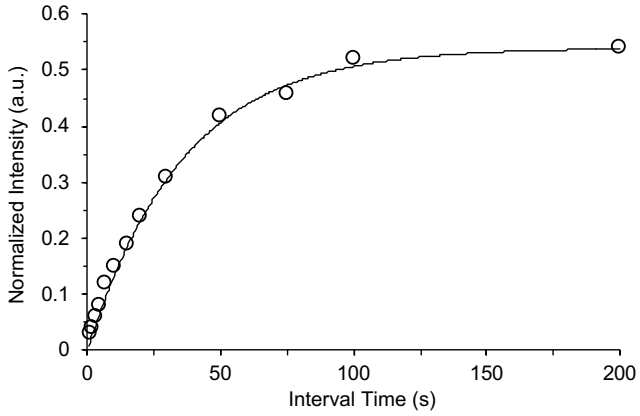

Fig. S8. Fitting of the ^{19}F spin-lattice relaxation time (T_1) of as-recrystallized **1** at 25 °C (T_1 = 35.8 s) using the saturation-recovery method (Larmor frequency = 376.17 MHz).

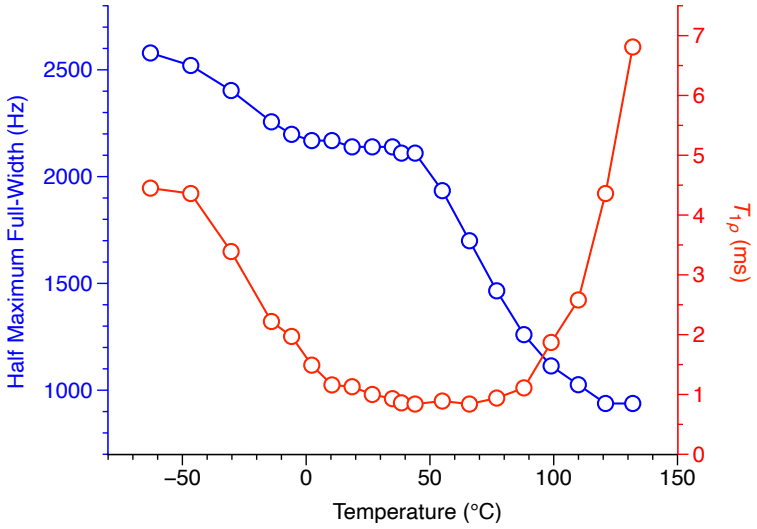

Fig. S9. Plots of full width at half maximum (Hz) of the ^{19}F-MAS NMR signal (blue) and $T_{1\rho}$ (red) *versus* temperature for thermally-treated **1** having a 2D+1D structure.

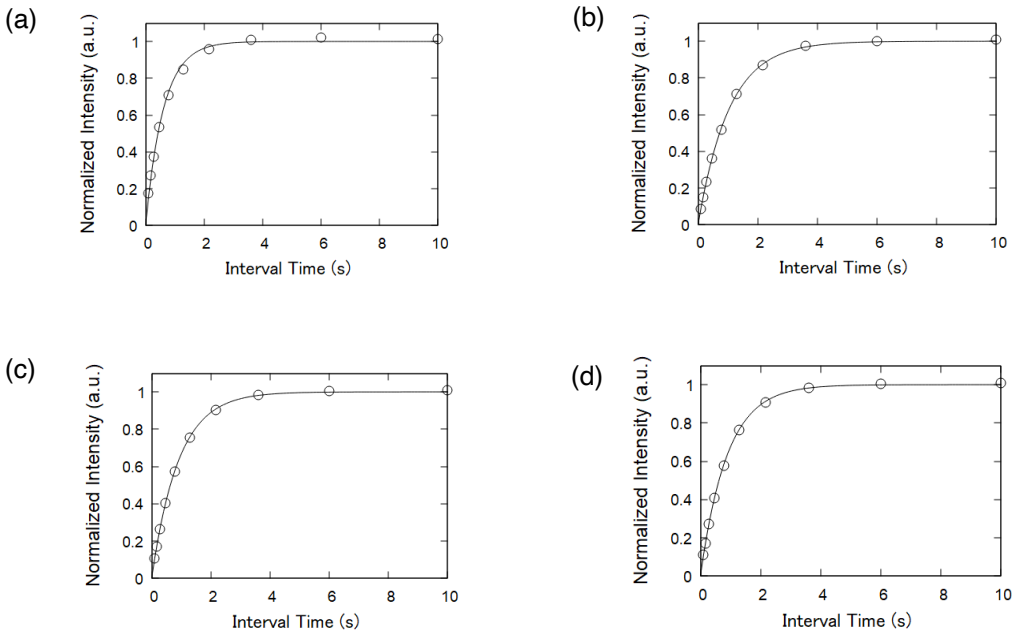

Fig. S10. Representative fittings of the ^{19}F spin-lattice relaxation time in the laboratory frame (T_1) for thermally-treated **1** having a 2D+1D structure at (a) –63 °C (T_1 = 0.67 s), (b) 10 °C (T_1 = 1.04 s), (c) 110 °C (T_1 = 0.90 s), and (d) 131 °C (T_1 = 0.93 s) using the saturation-recovery method (Larmor frequency = 470.62 MHz).

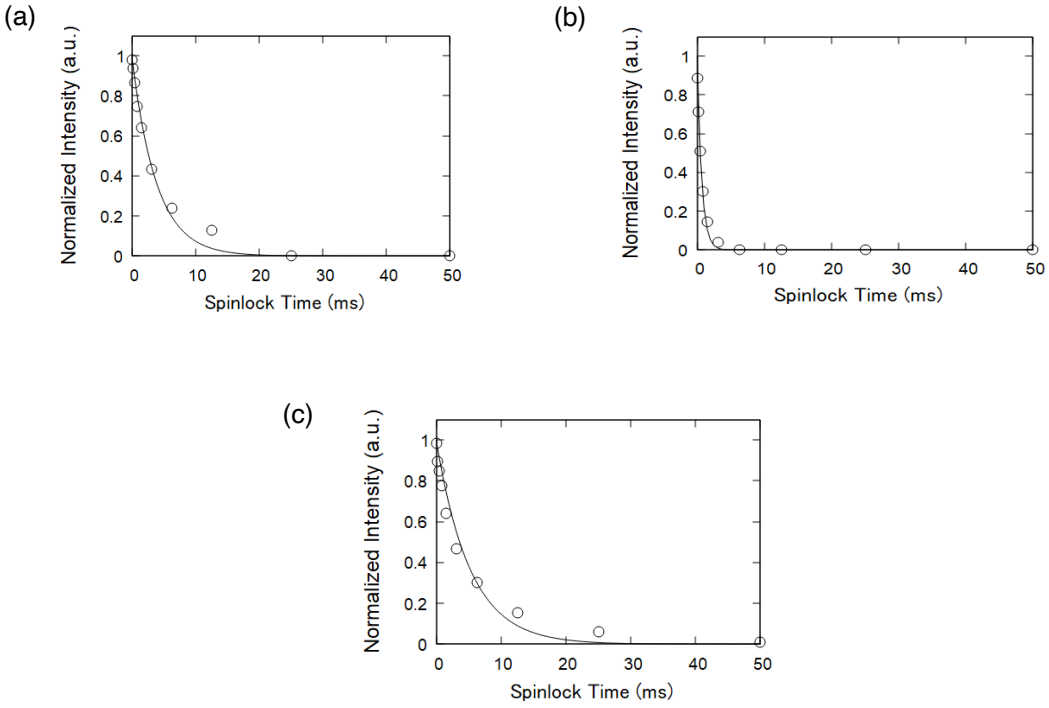

Fig. S11. Representative fittings of the ^{19}F spin-lattice relaxation time in the rotating frame ($T_{1\rho}$) for thermally-treated **1** at (a) –63 °C ($T_{1\rho}$ = 4.45 ms), (b) 66 °C ($T_{1\rho}$ = 0.84 ms), and (c) 131 °C ($T_{1\rho}$ = 6.81 ms) using the spin-lock method (Spinlock frequency = 50 kHz).

8. Supplementary tables

Table S1. Peak assignments for the VT-XRD profiles (Figs. 4 and S7) of **1**.

Process	Symbol	Temperature (°C)	d_{001} (nm)	d_{002} (nm)	d_{003} (nm)	d_{004} (nm)	d_{005} (nm)	d_{006} (nm)	d_{007} (nm)	d_{100} (nm)	d_{008} (nm)	d_{110} (nm)	d_{111} (nm)	d_{200} (nm)	d_{201} (nm)	*a* (nm)	*c* (nm)
1st heating	▲	230	5.2056	2.6051	1.7383	1.3022	1.0416	0.8685	0.7437	0.7099	0.6505	0.4110	0.4092	0.3567	0.3538	0.8214	5.2059
1st cooling	▲	225	5.1896	2.5900	1.7281	1.2968	1.0370	0.8649	0.7410	0.7082	0.6482	0.4103	0.4075	0.3560	0.3525	0.8190	5.1860
1st cooling	▲	190	5.1660	2.5802	1.7222	1.2922	1.0342	0.8617	0.7385	0.7041	0.6461	0.4080	0.4052	0.3537	0.3506	0.8142	5.1687
1st cooling	▲	160	5.1211	2.5531	1.7043	1.2782	1.0228	0.8517	0.7304	0.6991	0.6384	0.4053	0.4023	0.3514	0.3481	0.8087	5.1093
1st cooling	▲	100	5.1009	2.5452	1.6985	1.2745	1.0199	0.8500	0.7287	0.6948	0.6370	0.4032	0.3997	0.3495	0.3458	0.8039	5.0974
1st cooling	▲	25	4.9052	2.4455	1.6344	1.2265	N.D.	N.D.	N.D.	0.6876	N.D.	0.3985	0.3964	0.3455	0.3431	0.7961	4.8966
2nd heating	●	100	5.0813	2.5449	1.6959	1.2724	1.0188	0.8485	0.7275	0.6937	0.6364	0.4021	0.3993	0.3488	0.3454	0.8026	5.0908
2nd heating	●	200	5.1836	2.5867	1.7252	1.2932	1.0353	0.8627	0.7395	0.7048	0.6468	0.4083	0.4057	0.3541	0.3510	0.8151	5.1747
2nd cooling	●	230	5.1578	2.5750	1.7183	1.2895	1.0309	0.8587	0.7362	0.7066	0.6440	0.4101	0.4067	0.3556	0.3519	0.8179	5.1519
2nd cooling	●	220	5.1576	2.5751	1.7183	1.2881	1.0307	0.8583	0.7360	0.7060	0.6439	0.4089	0.4066	0.3546	0.3517	0.8166	5.1509
2nd cooling	●	200	5.1390	2.5688	1.7145	1.2855	1.0287	0.8566	0.7345	0.7035	0.6425	0.4077	0.4048	0.3538	0.3502	0.8138	5.1401
2nd cooling	●	160	5.1212	2.5546	1.7049	1.2781	1.0228	0.8517	0.7305	0.6991	0.6384	0.4053	0.4023	0.3514	0.3481	0.8087	5.1096
2nd cooling	●	100	5.1012	2.5453	1.6984	1.2744	1.0203	0.8500	0.7287	0.6947	0.6370	0.4032	0.3997	0.3496	0.3458	0.8040	5.0973
2nd cooling	●	25	4.9047	2.4456	1.6351	1.2261	N.D.	N.D.	N.D.	0.6878	N.D.	0.3966	N.D.	0.3455	0.3427	0.7951	4.8982

N.D. = Not detected

Table S2. Fitting parameters for thermally-treated **1** having a 2D+1D structure using the T_1 Kubo-Tomita functions[S12] (Fig. 7a): $1/T_1 = C\,[\tau_c/(1+\omega_0^2\tau_c^2) + 4\tau_c/(1+4\omega_0^2\tau_c^2)]$, $\tau_c^{-1} = \tau_0^{-1}\exp(E_a/RT)$, where ω_0, τ_0, R and T, are the spectrometer frequency (470.62 MHz), preexponential factor, gas constant (8.31 J K^{-1} mol^{-1}), and measurement temperature, respectively.

	C (s^{-2})	τ_0 (s)	E_a (kcal/mol)	Coefficient of Determination
Red Function	2.7×10^{8}	9.0×10^{-8}	3.3	−
Blue Function	4.5×10^{8}	2.1×10^{-7}	2.0	−
Black Function (Total)	−	−	−	0.951

Table S3. Fitting parameters for thermally-treated **1** having a 2D+1D structure using the $T_{1\rho}$ Kubo-Tomita functions[S12] (Fig. 7b): $1/T_{1\rho} = C\,[\tau_c/(1+\omega_0^2\tau_c^2) + 4\tau_c/(1+4\omega_0^2\tau_c^2)]$, $\tau_c^{-1} = \tau_0^{-1}\exp(E_a/RT)$, where ω_0, τ_0, R and T, are the spinlock frequency (50 kHz), preexponential factor, gas constant (8.31 J K^{-1} mol^{-1}), and measurement temperature, respectively.

	C (s^{-2})	τ_0 (s)	E_a (kcal/mol)	Coefficient of Determination
Red Function	2.2×10^{7}	9.0×10^{-2}	5.7	−
Blue Function	2.1×10^{7}	1.0×10^{-1}	5.5	−
Black Function (Total)	−	−	−	0.911